APPLICATION OF MAGNETIC SUSPENSION AND BALANCE SYSTEMS TO HYPERSONIC WIND TUNNEL TESTING

Andrew K. Owen
Department of Engineering Science
University of Oxford
Oxford, UK

SUMMARY

Wind tunnel model sting and shroud interference effects can be significant especially when testing small slender models which are required to simulate higher Knudsen number flows. Indeed, the presence of a sting of any size complicates all flowfield calculations since the model/sting geometry must also be numerically modeled.

Thus, in an attempt to generate reliable low density aerothermodynamic data on test models in flows closer to the flight test ideal, the University of Oxford Low Density Wind Tunnel was recomissioned for an extensive series of experiments in which a magnetic suspension and balance system was used to obtain sting and shroud free model data. Test data were obtained over wide ranges of freestream Mach (M= 6 - 9) Knudsen numbers (.001-0.3) on a wide variety of half angle cones at angle of attack, axially aligned cylinders of varying aspect ratio, and a model of the NASA Aerobrake vehicle.

In this paper, the critical components and functions of the magnetic suspension and balance system along with the levitation and test measurement procedures will be described. Techniques used to achieve model stability through the active control of lift, pitch and drag, and lateral stability, including suitable shaping of the magnetic field, and strategic placement of ferromagnetic material within the test section will be discussed. Coil placement, coil current control loop, and the interactive magnetic field and optical control procedures required for successful levitation will also be described. Details of the optical model position detection and feedback system which were developed for both conical and axisymmetric model levitation and testing will also be presented along with the procedures developed for drag calibration and measurement. Some of the data that were acquired during the program will also be presented and they include: Aerodynamic heat transfer and recovery factor measurements on slender cones, and the drag data obtained for the NASA Aerobrake vehicle.

MAGNETIC SUSPENSION SYSTEM DESCRIPTION

The Oxford University magnetic suspension and balance system in its basic form was designed and built by Haslam-Jones ('78) to measure cone drag in the Oxford University Low Density Wind Tunnel (Figure 1).

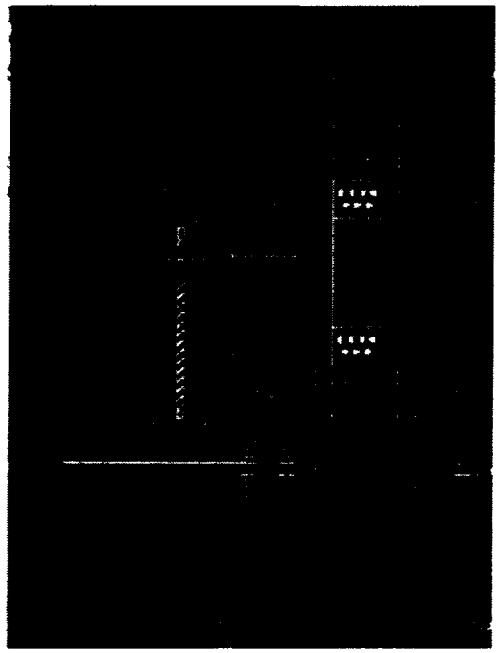

Figure 1 Magnetic Suspension System and Traversing Mechanism

A view of a levitated cone is shown in Figure 2. This view is looking at an angle of 45° towards the upstream direction with the cone in the centre of the test section. There was active control of lift pitch and drag, together with an inherent lateral stability due to suitable shaping of the magnetic field. This shaping was performed by the strategic placement of a ferromagnetic material within the test section resulting in a component of field towards the centre of the test section. This material can be seen at the corners of test section in Figure 2. The drag coils were split into front coils and rear coils which typically had 30 amps divided between them.

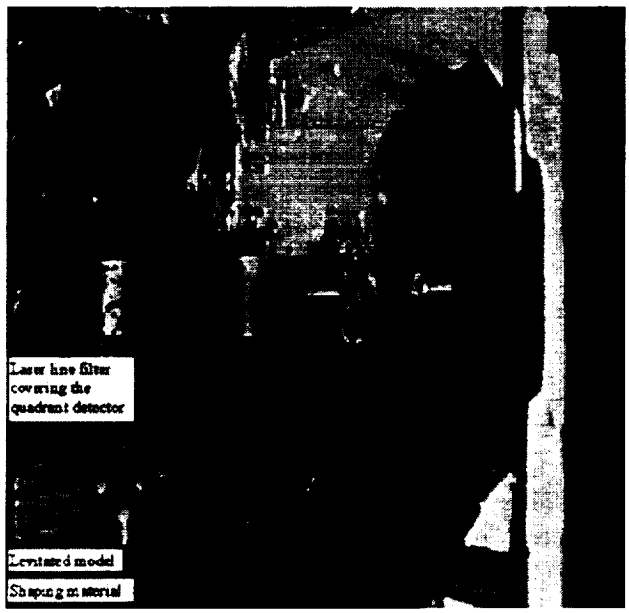

Figure 2 Cone Levitated in Test Section

They are located around the test section and were used to magnetise the model and maintain its axial location. The difference between the front and rear drag coil currents produced an axial gradient of the axial field component, while maintaining constant magnetisation of the model. With the drag coils magnetising the model, the lift and pitch coils, all located on the same horseshoe shape steel core, acted on the model as a magnetic dipole (Figure 3).

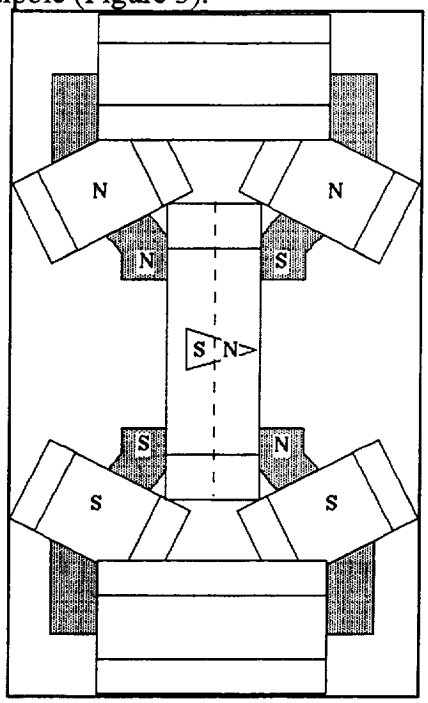

Figure 3 Magnetic fields

The pitch coils produced a uniform vertical field creating a pitching moment and the lift coils superimposed a horizontal gradient on this vertical field component to produce lift. The magnetic fields were controlled by Proportional, Integral, Differential (PID) analogue electronics with feedback provided by optical detection of the model position.

Within the vacuum chamber there is no effective inherent cooling other than radiation, therefore all of the magnetic coils were enclosed in water tight casings, and cooling water was continuously flowing through the system, preventing the coils from overheating.

This basic magnetic field coil construction was built by Haslam-Jones, as already mentioned, and essentially remained unaltered. In addition, the PID electronics was also that originally employed. However, the model detection system was completely renewed in order to perform the more advanced experiments undertaken by the author. This was made possible due to the new opto-electonic devices now available.

OPTICAL DETECTION SYSTEM

The original optical detection system consisted of 4 individual photodiodes arranged in the pattern shown in Figure 4.

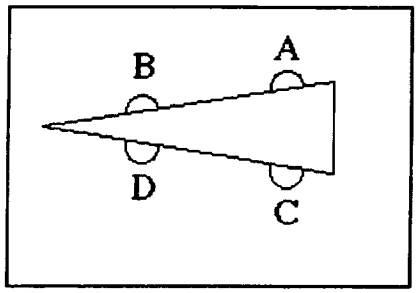

Figure 4 Original Detection System

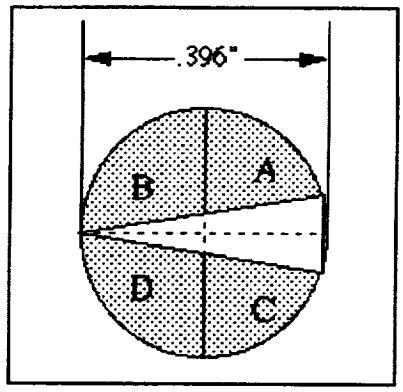

Figure 5 Modified Detection System

The physical size of the photodiodes restricted the size of cones which could be suspended. By replacing the existing 4 photodiodes with one quadrant photodiode, there was virtually no restriction on the minimum model size (Figure 5), and since the new detector worked in the same manner as the original individual photodiodes, no complex modification of the control circuits was required. The original incandescent light source was replaced with a low power (1 mWatt) class III laser diode (λ = 570 nM), and the quadrant detector was covered by a laser line filter, which eliminated the interference from ambient light which was a problem with the original incandescent light source. Since the laser diode is a source of unvarying light intensity, there was no longer a requirement to monitor the light intensity.

The laser beam traversed through the test section and over the model by a series of mirrors as shown in Figure 6. The model position was found by comparing the signals of the quadrant detector illuminated by the laser.

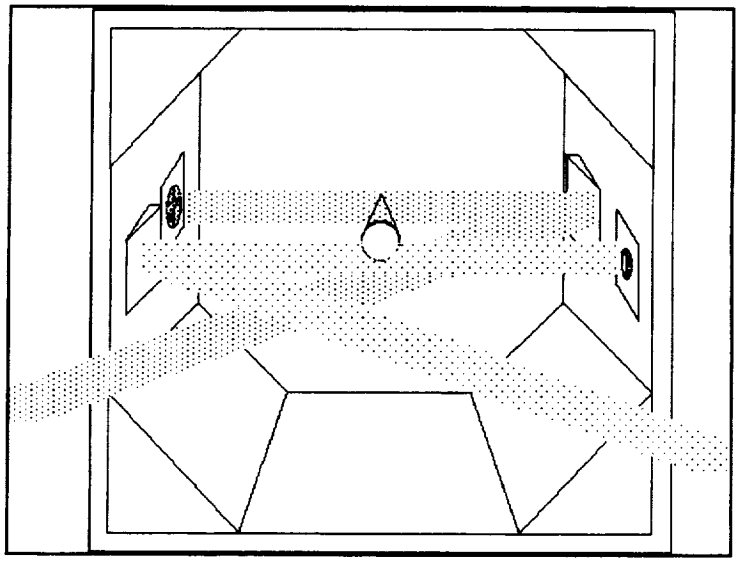

Figure 6 Test Section

Using the notation in Figure 5, the model was said to be in the null position when there was an equal signal from all four quadrants. This position was set by placing the model in approximately the right position and adjusting the potentiometers associated with each quadrant until equal outputs were observed. Axial movement of the model affected all four quadrants similarly, ie backward movement showed an increase in light signal on all four, while a forward movement showed a decrease in light level. For solely vertical movement, the outputs of the two lower quadrants were equal as were the

outputs of the two upper diodes, ie upward movement decreases the signal from the top two diodes, while increasing the lower ones. Pitching caused opposite pairs to behave the same way, ie pitching upwards caused the output of the front top quadrant and the rear bottom quadrant to decrease, with the output of the other two diodes increasing. The original control signals were as follows:

Drag	A + B + C + D + E
Lift	(A+ B+ 5E) - (C + D)
Pitch	(B + C + 5E) - (A + D)

The fifth diode (E) was used to monitor the overall light level intensity, and was replaced with a constant voltage signal since the laser is a source of essentially constant intensity.
The additional benefit of this new system is that it enables position detection

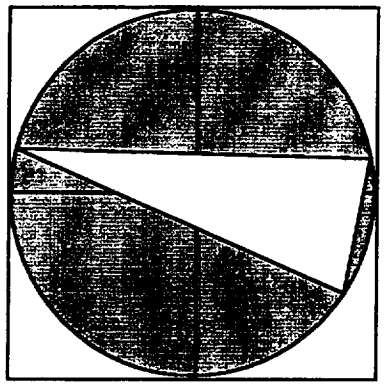

Figure 7 Model at Non-Zero Angle of Attack

of cones at non-zero angles of attack. Figure 7 shows the orientation of a model at non-zero angle of attack. Following the nomenclature of Figure 5, and the control signals described above, it can be seen that the same criteria apply. The maximum angle of attack was therefore limited by the pitch coil current distribution. This distribution is discussed in the appendix on the operational procedure of the Magnetic Suspension System.

NON-CONICAL MODELS

The optical system also has a removable second laser diode, and single photodiode detector for use with non-conical models (Figure 8).

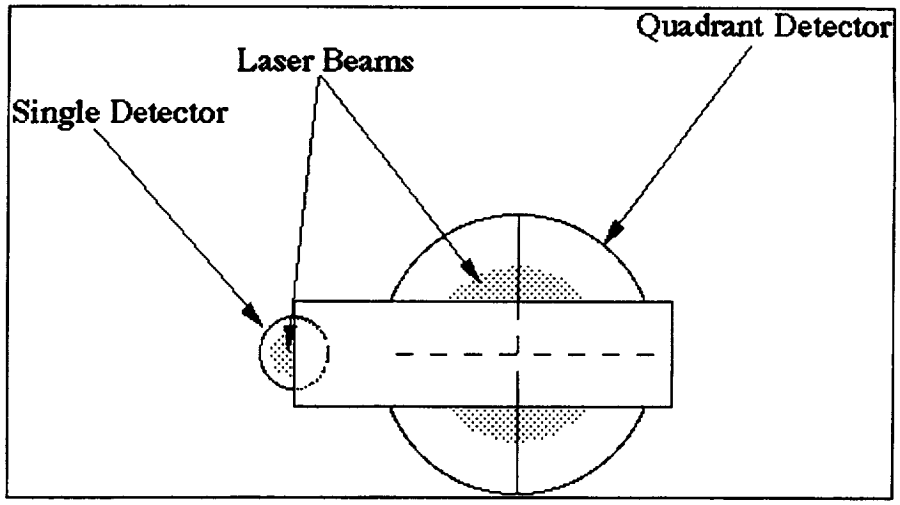

Figure 8 Non-Conical Model Position Sensing

This additional system was used to detect the rear of the model and replaced the above mentioned drag control signals with the output from the single photodiode.

MODEL STABILITY

The Magnetic Suspension System has active control of drag lift and pitch. There was no active control of yaw, roll, or lateral position. Yaw was stabilised by the drag coils creating a field in the axial direction. This field induces a moment and magnetic field within the model which produced a stabilising yaw moment if the model axis was misaligned with the balance axial directiion. Roll was seen to be of little consequence to the bodies of revolution tested, and was, therefore, not controlled at all. However, roll could be used to determine viscous terms by monitoring the roll speed as a function of time whilst the model was suspended. The lateral position was maintained by suitable shaping of the axial magnetic field. By placing ferromagnetic material in strategic positions in the test section, a component of force was created towards the centre.

CALIBRATION TECHNIQUE

The magnetic suspension and balance system is used to measure the aerodynamic forces applied to a model under test conditions. The forces on a suspended model are balanced by the magnetic force required to hold the model in a stationary position relative to the flow. This magnetic force comes about from a change in the distribution of current in the two drag coils. A calibration procedure is required to relate the coil currents to the forces applied to a model. Previously, the calibration procedure entailed glueing the end of a light thread to a model and then tying small weights to the other end which was draped over a pulley, thus applying an axial force on the model. This procedure is quite straightforward and, although laborious, produces a fairly accurate calibration. The drawbacks are that this technique inevitably suffers from the effects of friction and pendulum movements of the hanging weights. A new technique was developed that has no errors due to friction.

The entire balance is tilted with a hydraulic jack so that the mass of the model itself is used in the calibration, both techniques are shown in Figure 9.

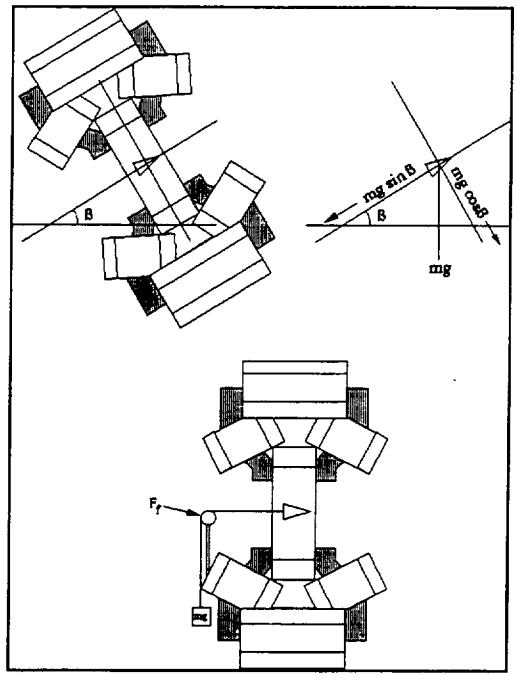

Figure 9 Calibration Methods

The angle to which the balance is rotated is measured on an inclinometer fixed to the balance and has an accuracy of one minute. The angle and the difference in the two drag coils are logged in the data acquisition system. The procedure is repeated at several different angles and a calibration is taken from the slope of the resulting line. A comparison of the two techniques is shown in Figure 10.

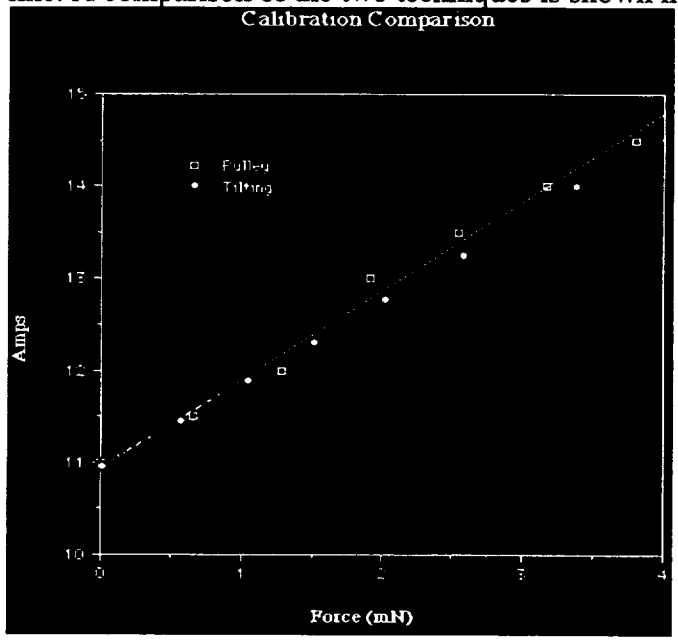

Figure 10 Calibration Comparison

It can be seen that there is a very small difference in the two procedures. However there is little scatter in the tilting calibration, and this procedure proved to be more practical.

A typical calibration done before and after a run is shown Figure 11, which demonstrates the repeatability of the drag calibration procedure.

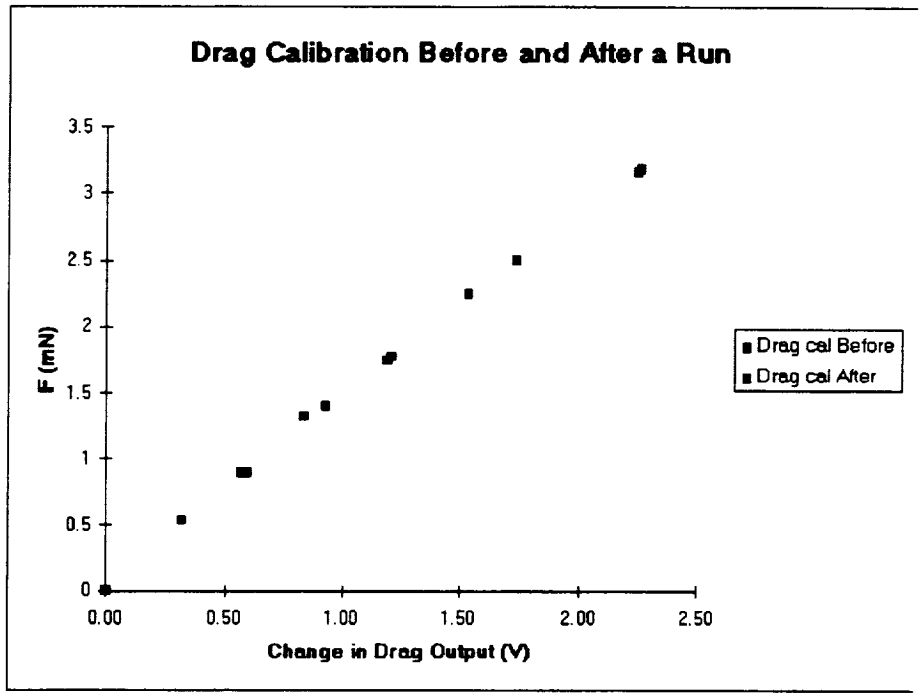

Figure 11 Drag Calibration Before and After a Run

A comparison of calibrations obtained for a cone at varying angle of attack is shown in Figure 12.

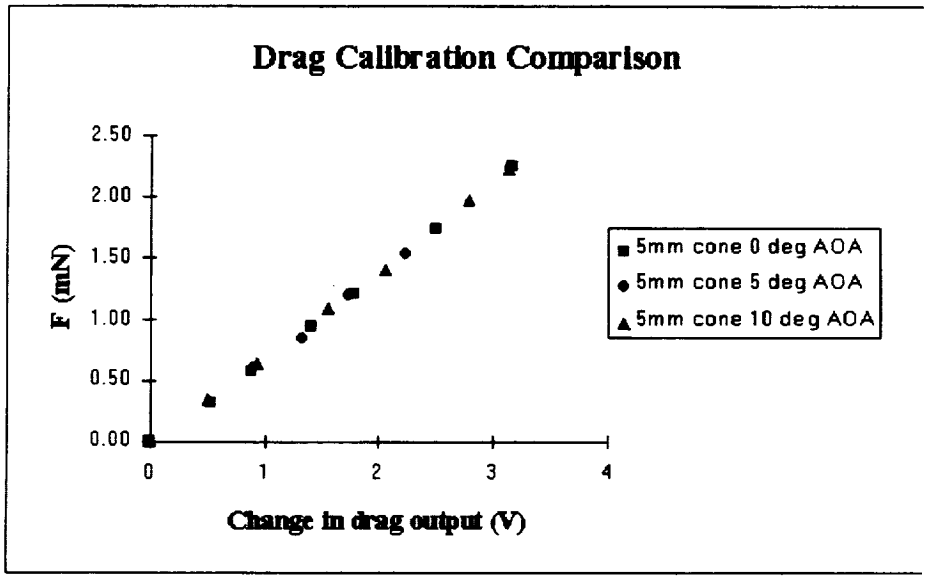

Figure 12 Calibration comparison of a cone at 3 different angles of attack

It can be seen that there is essentially no difference in the calibration with the different angles of attack. This was taken to be true on all subsequent testing of cones at angles of attack.

HEAT TRANSFER AND RECOVERY TEMPERATURE MEASUREMENTS

The total heat transfer and recovery temperature of a cone have been measured while the model was suspended. The heat transfer was to be measured using calorimetry techniques whereas the recovery temperature was found from the equilibrium temperature. The model temperature was measured remotely utilising liquid crystals.

The following technique was used to measure the convective and radiative heat transfer rates using the temperature sensitive liquid crystals. The model temperature was measured by observing the colour of the liquid crystal on the cone as previously stated. The model was suspended in the magnetic balance and then heated in a vacuum to a temperature above the colour play of the liquid crystals. The cone models had a good thermal conductivity so their internal temperature was essentially uniform and the models acted as calorimeters. With the test section at the operating background pressure and with no flow established, the heater was removed and the model was allowed to cool radiatively. Using the liquid crystal calibration, a comparison was made with the cooling experiment to determine accurate model temperature. With this procedure it was possible to obtain a history of model temperature against time, Figure 13. With a relatively simple analysis, the radiative and convective heat transfer coefficients can be calculated.

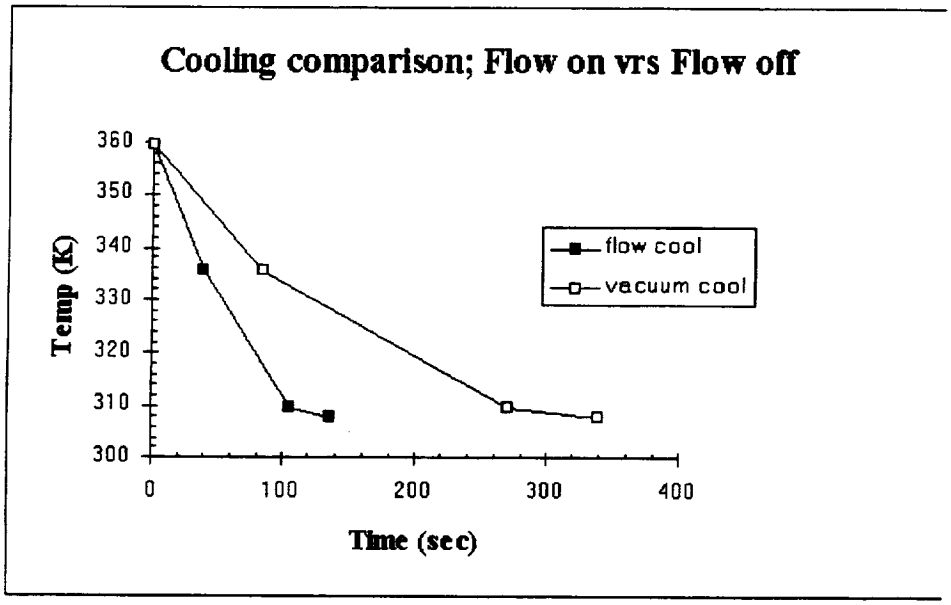

Figure 13 Cooling Rates

A technique for determining the recovery temperature of a levitated cone has also been developed. The procedure involves coating the model with temperature sensitive liquid crystals having colour play temperatures around those of the expected recovery temperature.

In the present experiments, the recovery factor for a 6.5 degree half angle silver steel cone has been found in a low density nitrogen flow at both zero incidence and at 10 degrees angle of attack in a Mach 5.4 flow. The cone base was covered with three temperature sensitive liquid crystals, with colour play temperatures of 10, 15, and 22 degrees C. The stagnation chamber was heated until the 22 degree crystal colour play had been exceeded so that the model temperature was above 25 degrees C. The flow stagnation chamber was then allowed to cool and the model temperature decreased accordingly. By monitoring the liquid crystal colour changes, along with the corresponding stagnation temperature, the recovery factor could be deduced. The model temperature corresponds to the colour of the liquid

crystals during their color play. A graph of stagnation temperature vs. model temperature is shown in Figure 14 for the two models tested at zero and 10° angles of attack (AOA).

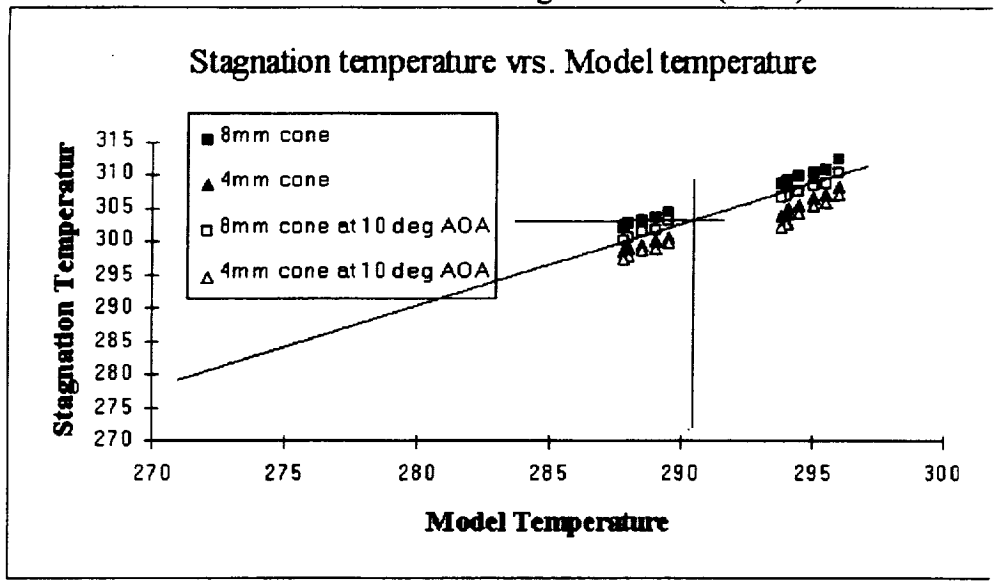

Figure 14 6.5 degree cone model cooling in heated Mach 5.4 flow

To find the recovery factor, shown in Figure 14, a point on the line where the model temperature is equal to the chamber wall temperature is taken. This is done so that there is no effect of radiation to or from the chamber wall.

NASA AEROBRAKE

Aero-assisted space transfer vehicles have three primary components: the aerobrake, the payload, and the propulsion unit. Flowfield interaction with and between these elements can have significant effects on drag, vehicle stability, and allowable payload size and shape. Of particular importance is the interaction of the near wake with the payload compartment. Consequently, precise determination of drag and wake structure are critical issues for aerobrake design. Unfortunately, the heating and aerodynamic forces which result from the interactions between the payload and the near wake are not well understood. Also, available experimental data are not sufficient for design purposes nor sufficient to validate CFD models. The few data which are available are contaminated to unknown degrees by sting or shroud interference or model wire suspension effects. In particular, the most recent direct simulation Monte Carlo (DSMC) calculations of Moss et al ('95) indicate that considerable sting/wake interference effects call into question conventional sting mounted model experimental data obtained in low density hypersonic wind tunnels at CNRS Meudon and DLR Gottingen. These data, generated in support of AGARD Working Group 18, are known to be influenced by model support interference. As a result, additional calculations are needed to explore the sensitivity of the wake to sting effects. Reliable experimental and prediction design methods will be essential to the success of future space missions. This will require new interference free test results which will provide unique test cases for the validation of DSMC calculations and predictions generated by solutions of the rarefied forms of the Navier-Stokes equations.

The University of Oxford magnetic balance and suspension system offers the opportunity to generate new aerothermodynamic drag and wake flow data in the rarefied flow regime on realistic space vehicle models and payload shapes.

The Aerobrake model used for testing is shown in Figure 15.

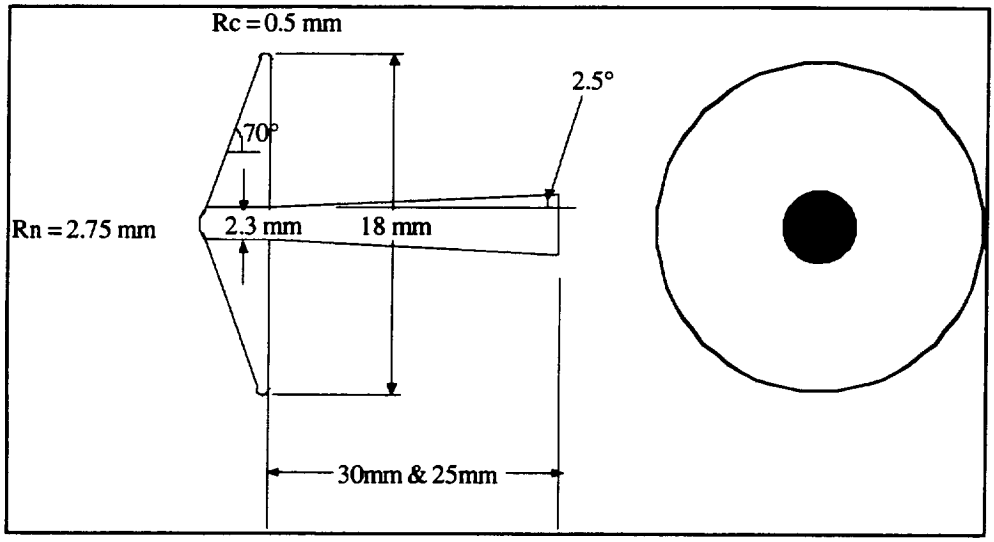

Figure 15 Aerobrake model

A 2.5 degree semi-angle afterbody was used with the aerobrake in order to maintain compatibility with the original optical detection system. The detection system was modified so that different afterbody model geometries can now be tested. However, for the tests undertaken, a series of drag measurements were obtained on the Aerobrake with two different afterbodies. The 25 and 30 mm afterbodies were 2.3 mm in diameter and attached to the

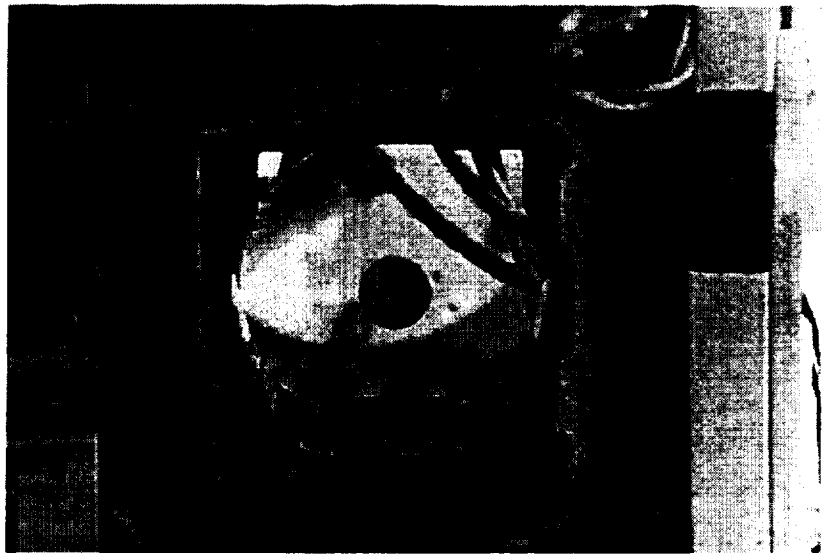

Figure 16 Aerobrake in Suspension

18 mm base diameter of the Aerobrake model. This more than satisfied the AGARD guidelines for sting interference, and set the Knudsen number, based on model base diameter, in the range between

0.005 and 0.01. The Aerobrake was made of a light non-feromagnetic material, balsa wood, and the afterbodies were constructed of mild steel. A picture of the Aerobrake in suspension can be seen in Figure 16. This view of the Aerobrake is taken from a downstream location through the test section. The present results of the drag on the Aerobrake are shown in Figure 17, and are compared with DSMC results of Gilmore et. al. ('94) for the same configurations. A unique feature is the decrease in Cd with increasing Kn, evident in both the experimental data and the DSMC predictions. This trend is opposite to that which has been experienced with the slender cones, and is attributed to a negative shear component acting along the sting. This shear component is a result of the recirculating region reattatching along the sting, and acts in an upstream direction. The trend could also be associated with an increase in base pressure.

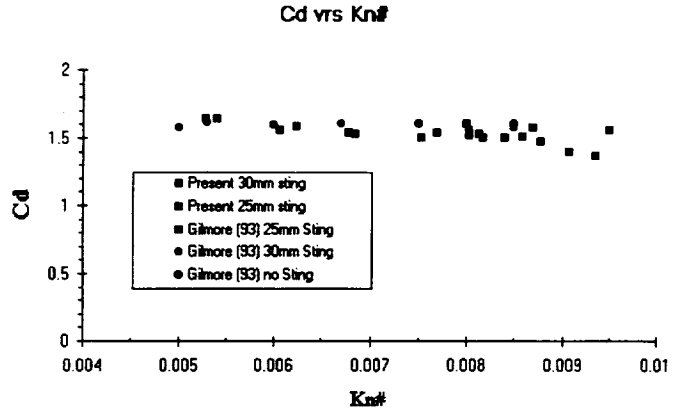

Figure 17 Experimental Aerobrake Drag Results Compared with DSMC Predictions

In Figure 18 the data are compared with Cd results for the Mars Pathfinder calculated from the data collected during its decent into the Martian atmosphere in July 1997.

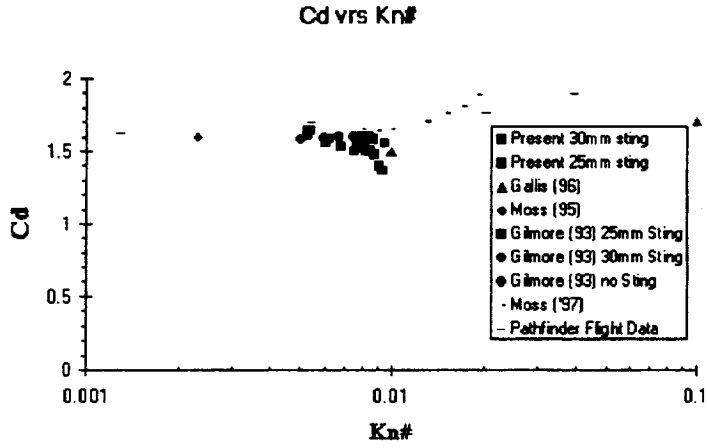

Figure 18 Experimental Aerobrake Drag Results Compared with Mars Pathfinder Flight Data

The decrease in Cd with increasing Knudsen number is also evident in the drag coefficient shown in Figure 19 computed from the Viking 1 pressure and acceleration data. Viking 1 also had a 70 degree blunt nose cone and entered the Martian atmosphere in June, 1976. This effect on Viking has been attributed, by NASA, to a departure from chemical equilibrium with the increase in altitude which results in a reduction in pressure coefficient and corresponding decrease in drag coefficient. This explanation was concluded in 1975 from experiments in the Langley Expansion Tube facility by C.

Miller, (Blanchford et. al. ('97)). At even higher altitudes rarefied-flow effects begin to dominate and Cd rises again.

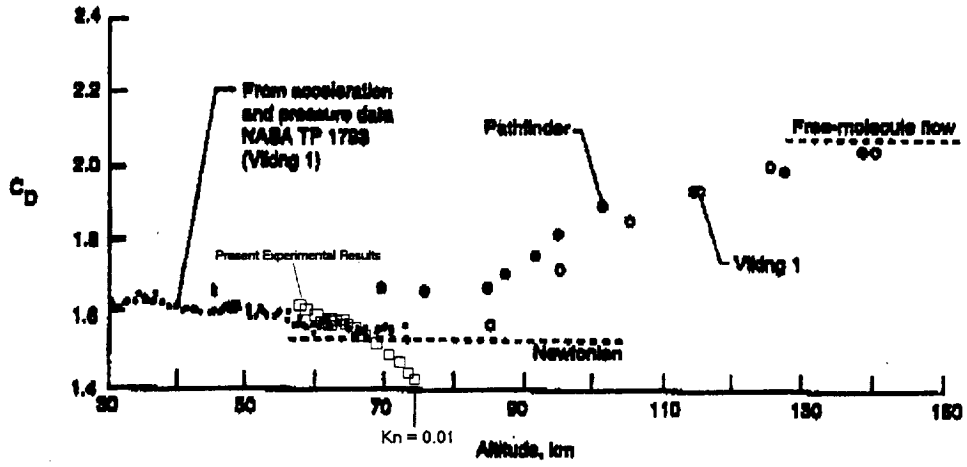

Figure 19 Viking 1 drag coefficient vs altitude from flight measurements and DSMC simulations along with Pathfinder drag coefficient predictions from DSMC simulations (from Blanchford et al '97) and including the present experimental results

The present data shows a decreasing Cd with increasing Kn over the range tested and this appears to be consistent with available flight data both from Pathfinder and Viking. The present experimental Cd values are a little below those of the CFD. However, this trend appears to be supported. The mechanism for the decrease is still the subject of investigation, although from the low enthalpy results here, and the CFD predictions, it does appear that it is more of an aerodynamic effect rather than an effect due to chemical non-equilibrium.

REFERENCES

1. Haslam-Jones, T.F. (1978) "*Measurements of the Drag of Slender Cones in Hypersonic Flow at Low Reynolds Numbers Using a Magnetic Suspension and Balance*," Oxford University Report 1235/78

2. Moss, J.N., Price, J.M., and Dogra, V.K.(1995) "*DSMC Calculations for a 70 degree blunted cone at 3.2 km/s in nitrogen,*" NASA TM 109181

3. Gilmore, M.R., Owen, A.K., and Jones, T.V. (1994) "*70° Aerobrake Vehicle plus Afterbody in Hypersonic Rarefied Nitrogen Flow*," Rarefied Gas Dynamics, 19th Symposium

4. Blanchard, R.C., Wilmoth, R. G., Moss, J. N. (1997) "*Aerodynamic Flight Measurements and Rarefied-Flow Simulations of Mars Entry Vehicles*," J. of Spacecraft and Rockets, Vol.34, No. 5